Unravelling the transcriptional responses of TGF-β: Smad3 and EZH2 constitute a regulatory switch that controls neuroretinal epithelial

THE FASEB JOURNAL • RESEARCH • www.fasebj.org

Unravelling the transcriptional responses of TGF-β: Smad3 and EZH2 constitute a regulatory switch that controls neuroretinal epithelial cell fate specification

Darrell Andrews,[*,†] Giorgio Oliviero,[‡] Letizia De Chiara,[§] Ariane Watson,[¶] Emily Rochford,[‖] Kieran Wynne,[‖] Ciaran Kennedy,[*,‖] Shane Clerkin,[*,‖] Benjamin Doyle,[‖] Catherine Godson,[*,†] Paul Connell,[†,#] Colm O'Brien,[†,#] Gerard Cagney,[‖] and John Crean[*,‖,1]

[*]Diabetes Complications Research Centre and [‖]University College Dublin (UCD) School of Biomolecular and Biomedical Science, Conway Institute of Biomolecular and Biomedical Science, [†]UCD School of Medicine and Medical Science, [‡]National Institute for Bioprocessing Research and Training, and [¶]Systems Biology Ireland, University College Dublin, Dublin, Ireland; [§]Department of Biomedical, Experimental, and Clinical Sciences, Centro di Eccellenza DeNothe, University of Florence, Florence, Italy; and [#]Department of Ophthalmology, Mater Misericordiae University Hospital, Dublin, Ireland

ABSTRACT: Cell differentiation is directed by extracellular cues and intrinsic epigenetic modifications, which control chromatin organization and transcriptional activation. Central to this process is PRC2, which modulates the di- and trimethylation of lysine 27 on histone 3; however, little is known concerning the direction of PRC2 to specific loci. Here, we have investigated the physical interactome of EZH2, the enzymatic core of PRC2, during retinoic acid–mediated differentiation of neuroepithelial, pluripotent NT2 cells and the dedifferentiation of neuroretinal epithelial ARPE19 cells in response to TGF-β. We identified Smad3 as an EZH2 interactor in both contexts. Co-occupation of the CDH1 promoter by Smad3 and EZH2 and the cooperative, functional nature of the interaction were established. We propose that the interaction between Smad3 and EZH2 targets the core polycomb assembly to defined regions of the genome to regulate transcriptional repression and forms a molecular switch that controls promoter access through epigenetic mechanisms leading to gene silencing.—Andrews, D., Oliviero, G., De Chiara, L., Watson, A., Rochford, E., Wynne, K., Kennedy, C., Clerkin, S., Doyle, B., Godson, C., Connell, P., O'Brien, C., Cagney, G., Crean, J. Unravelling the transcriptional responses of TGF-β: Smad3 and EZH2 constitute a regulatory switch that controls neuroretinal epithelial cell fate specification. FASEB J. 33, 6667–6681 (2019). www.fasebj.org

KEY WORDS: PRC2 · differentiation · chromatin · interactome

TGF-β is widely accepted to play a key pathogenic role in many disease processes (1). In epithelial cells, TGF-β can induce partial or full transdifferentiation into mesenchymal cells through the process of epithelial-to-mesenchymal transition (EMT). This was first demonstrated during embryonic development and subsequently received a huge amount of interest in diverse disease processes including cancer, cardiovascular disease, and diabetes. [For a review, see ref. (2)]. Significant efforts have been made to target TGF-β for the treatment of many diseases, with little success to date. At the core of this issue remains a fundamental gap in our knowledge of how TGF-β signaling regulates gene expression. Potential new approaches are emerging from recent studies examining the role of TGF-β during embryonic development, coupled with the identification of similar, parallel processes in adult tissues (3, 4). TGF-β acts mainly though the activation of Smad2 and Smad3 transcription factors (5), and these recent studies revealed that Smad-mediated transcriptional responses are regulated by master transcription factors in embryonic stem cells (ESCs) and interact with the general chromatin machinery. Novel interactions between Smads, transcriptional repressors and activators, and chromatin-modifying complexes such as the polycomb group (PcG) proteins are proposed to regulate the balance between self-renewal and specification. Therefore, a combination of DNA sequence, chromatin environment, cellular context, and signaling dictate genome wide events. [For a review, see ref. (6)]. However, little is known about the molecular mechanisms by which

ABBREVIATIONS: ChIP-seq, chromatin immunoprecipitation sequencing; dsRNA, double-stranded RNA; DZnep, 3-deazaneplanocin A; EMT, epithelial-to-mesenchymal transition; ESC, embryonic stem cell; esiRNA, endoribonuclease-prepared siRNA; GAPDH, glyceraldehyde-3-phosphate dehydrogenase; GFP, green fluorescent protein; H3, histone 3; iBAQ, intensity-based absolute quantification; miR302, microRNA 302; PcG, polycomb group; siRNA, small interfering RNA

[1] Correspondence: Diabetes Complications Research Centre, UCD School of Biomolecular and Biomedical Science, Conway Institute of Biomolecular and Biomedical Science, University College Dublin, Belfield, Dublin 4, Ireland. E-mail: john.crean@ucd.ie

doi: 10.1096/fj.201800566RR
This article includes supplemental data. Please visit *http://www.fasebj.org* to obtain this information.

signaling pathways direct epigenetic changes of genes responsible for differentiation, in particular, the role that histone modifications may play in this process.

Epigenetic mechanisms that regulate access to the genetic material *via* histone methylation are critical for determining gene expression during fate specification and embryonic development. Specifically, methylation of lysine 27 of histone 3 (H3) (H3K27me3) by the enzymatic components of PRC2, EZH1, and EZH2 (7, 8) leads to a transcriptionally repressive state, which can be reversed by the action of Jumonji C domain–containing histone demethylases. Indeed, the balance between methyltransferase and demethylase activity is widely accepted to regulate repression and derepression of many key developmental promoters. In bivalent promoters marked with both repressive (H3K27me3) and active (H3K4me3) histone post-translational modifications (9), PcG complexes hold the poised RNA polymerase II at transcriptional start sites, thereby inhibiting its release (10). In addition, PcG complexes can compact chromatin, thereby blocking the accessibility of chromatin-remodeling machinery, which is required during transcription activation. In the context of TGF-β signaling, the cooperative binding of Smad3 and JMJD3 has been shown to control many aspects of neural specification (11); however, little is known about how the polycomb repressive complex can be targeted to *cis*-regulatory elements to facilitate repression. It has been proposed that transient interactions with transcription factors can mediate the recruitment of polycomb repressive complexes to DNA-specific sequences. Notably, Smad3 was recently shown to interact with the histone lysine methyltransferase SETDB1 to regulate the epitranscriptome during fate specification (12) and in response to TGF-β (13).

We recently demonstrated that silencing of the TGF-β type II receptor promotes the acquisition of plasticity, suggesting that TGF-β signaling to chromatin plays a critical role in determining cell fate decisions in adult cells (14–16). Here we demonstrate, for the first time, an interaction between Smad3 and EZH2, the enzymatic component of the PRC2 complex, during neuroepithelial cell differentiation and TGF-β mediated neuroepithelial dedifferentiation, and we elaborate on possible functional roles of this complex. We hypothesize that this complex targets the core polycomb assembly to defined genomic regions, regulating transcriptional repression and forming a molecular switch that controls promoter access through epigenetic mechanisms leading to gene silencing.

MATERIALS AND METHODS

Cell culture and differentiation of NT2 and retinal pigment epithelium cells

Human retinal pigment epithelial cells, ARPE19 (CRL-2302; American Type Culture Collection, Manassas, VA, USA) were cultured in DMEM F12 Hams (MilliporeSigma, Burlington, MA, USA) supplemented with 10% (v/v) fetal bovine serum, 2 mM L-glutamine, and 100 U/ml of penicillin per one milligram per milliliter streptomycin (all from Thermo Fisher Scientific, Waltham, MA, USA). Cells were maintained in a humidified 5% CO_2, 37°C atm. To induce epithelial dedifferentiation, cells were growth arrested for 24 h in restriction medium of DMEM-F12 Hams containing 100 U/ml penicillin, 100 μm/ml streptomycin, and 2 mM L-glutamine only. Human recombinant TGF-β_2 (PromoCell, Heidelberg, Germany) was added to the medium at a final concentration of 5 ng/ml for 24–72 h. NT2/D1 cells (CRL-1973; American Type Culture Collection) were cultured and differentiated as previously described (17).

Viral transduction of ARPE19 cells

For viral transduction, cells were seeded at a density of 5×10^4 cells per well in a 6-well plate. The following day, the cells were transduced with a polycistronic lentiviral vector encoding all 4 members of the microRNA 302 (miR302) family as well as green fluorescent protein (GFP) (miR302a, -b, -c, and -d) (Systems Biosciences, Palo Alto, CA, USA) or a control virus containing a scrambled sequence (pGIPZ) (Thermo Fisher Scientific). Nontransduced cells were maintained in parallel as a control. The medium was changed every 2 d. For TGF-β treatment experiments, cells were serum starved on d 6 post-transduction as outlined above, followed by treatment with TGF-β on d 7 at the appropriate time points. For long-time course experiments, cells were reseeded on d 7 and 14 at a ratio of 1:5 to 1:7. Both the miR302 vector and the scrambled pGIPZ contain a GFP reporter gene under the control of the same promoter as the insert of interest; therefore, successful transduction was verified by examining the percentage of GFP-positive cells.

Plasmids and transfection

Plasmid constructs pCMVHA EZH2 (24230), pRK5F Smad3 (12625), and pro-E-cad670-Luc (42083) were from the Addgene plasmid repository (Watertown, MA, USA). Transient transfections were carried out using Fugene HD transfection reagent (Promega, Madison, WI, USA) diluted in Opti-Mem-1 medium (Thermo Fisher Scientific) according to the manufacturer's instructions, using a ratio of 1:3 of DNA to transfection reagent.

Knockdown of Smad3 and EZH2

Small interfering RNA (siRNA) was prepared with endoribonuclease (esiRNA) essentially as described by Heninger and Buchholz (18) with some modifications. Briefly, cDNA was isolated from NT2 cells to use as a template for the generation of T7 promoter–flanked cDNA fragments through 2 rounds of PCR amplification. The resulting fragments contained the mRNA region against which the esiRNAs would target their gene of interest. These fragments were then transcribed *in vitro* to generate double-stranded RNA (dsRNA) of the target amplicons. These were subsequently purified to isolate fragments >250 bp. After purification, dsRNA was digested with an E38A RNase III mutant purified from *E. coli* to generate a pool of ~21 nt siRNAs. siRNA fragments were then purified using an RNeasy Kit (Qiagen, Germantown, MD, USA) to remove any undigested, larger dsRNA from the pool, followed by a final purification to remove any contaminants. The primers used to generate these esiRNAs can be found in **Table 1**.

For knockdown experiments, 6×10^5 ARPE19 cells were seeded into 6-well tissue culture plates. Cells were transfected in suspension immediately after seeding with 742 ng of purified esiRNA pools against Smad3 and EZH2 or a scrambled control using 4.45 μl of Lipofectamine 2000 reagent (Thermo Fisher Scientific) diluted in Opti-Mem-1 medium (Thermo Fisher Scientific). Sixteen hours after transfection, the medium was changed to serum-free medium. TGF-β was added to the medium 48 h

TABLE 1. *Primer sequences for esiRNA synthesis*

Gene	Primer sequence, 5′–3′	
	Forward	Reverse
eGFP	CCACATGAAGCAGCACGA	CGTCCTCGATGTTGTGGC
EZH2	GAGGACGGCTTCCCAATAAC	GGAGCTGGAGCTATGATGCTA
SMAD3	ACAAGGTCCTCACCCAGATG	TGGACTGTGACATCCCAGAA

Primer sequences denote target gene only. eGFP, enhanced GFP.

after transfection, and cells were harvested for Western blot analysis 48 h after addition of TGF-β.

Reagents and antibodies

Human recombinant TGF-β_2 was purchased from PromoCell. All-*trans*-retinoic acid was purchased from MilliporeSigma. Antibodies used in Western blot analysis, immunoprecipitation, and chromatin immunoprecipitation can be found in **Table 2**. Rhodamine phalloidin and DAPI were from Thermo Fisher Scientific. Anti-mouse or anti-rabbit horseradish peroxidase–labeled secondary antibodies were from Cell Signaling Technology (Danvers, MA, USA). 3-Deazaneplanocin A (DZnep) was purchased from Calbiochem (San Diego, CA, USA), and SB431542 was purchased from Merck (Darmstadt, Germany).

Protein extraction and Western blot analysis

For whole cell lysis, protein extracts were prepared in radio immunoprecipitation lysis buffer [50 mM Tris-HCl pH 7.5, 150 mM NaCl, 0.25% sodium deoxycholate, 1 mM EDTA, and 1% IGEPAL, supplemented with protease and phosphatase inhibitor cocktails (MilliporeSigma)]. After incubation at 4°C for 30 min, cellular debris was removed by centrifugation at 12,000 *g* for 15 min at 4°C, and the cleared supernatant was transferred into a new tube and stored at −20°C. For nuclear fractionation, cells were resuspended in ice-cold hypotonic buffer [10 mM HEPES, 1.5 mM $MgCl_2$, 10 mM KCl, 0.5 mM DTT, and 10% glycerol, supplemented with protease and phosphatase inhibitor cocktails (MilliporeSigma)]. After incubation on ice for 15 min, cell membranes were mechanically disrupted using a Dounce homogenizer with a loose piston. The samples were centrifuged for 5 min at 5000 rpm, and the supernatant containing the cytoplasmic fraction was transferred to a new tube and stored at −80°C. The nuclear pellet was stored at −80°C until required.

Protein concentration was quantified by Bradford assay (Bio-Rad, Hercules, CA, USA) according to standard procedures. Samples were resolved by 10–12% SDS-PAGE, transferred to a PVDF membrane (MilliporeSigma), and blocked for 1 h in PBS containing 0.1% Tween 20 and 5% (w/v) skimmed milk. Membranes were incubated overnight with primary antibody at 4°C in blocking buffer before incubation with horseradish peroxidase–conjugated secondary antibody at room temperature for 1 h. Chemiluminescent detection using Western Bright ECL/Quantum/Sirus (Advansta, San Jose, CA, USA) allowed for visualization of the protein bands.

Endogenous immunoprecipitation

Endogenous immunoprecipitations were performed on nuclear lysates extracted as outlined above. Anti-EZH2 antibody (kind gift from Dr. Adrian Bracken, Trinity College Dublin, Dublin, Ireland) was coupled to 50 μl of packed Protein A beads (MilliporeSigma) overnight by incubating in 1 ml of PBS containing 0.1% Tween 20. Beads were collected by centrifugation at 2000 rpm for 1 min. The beads were washed twice with 1 ml of 0.2 M sodium borate pH 9.0. The antibody was then cross-linked to the beads by incubating with 20 mM dimethyl pimelimidate dihydrochloride in 0.2 M sodium borate pH 9.0 for 30 min rotating at room temperature. The reaction was quenched by washing the beads with 1 ml of 0.2 M ethanolamine pH 8.0 followed by incubation with 1 ml of 0.2 M ethanolamine for the 2 h at room temperature. Beads were then washed twice with PBS containing Tween 20 and blocked for at least 1 h at 4°C rotating in blocking buffer [0.2 mg/ml chicken egg albumin (MilliporeSigma), 0.1 mg/ml insulin (MilliporeSigma), and 1% fish skin gelatin (MilliporeSigma) in Buffer B]. Buffer B consisted of 20 mM

TABLE 2. *Antibodies used in Western blot, immunoprecipitation, and chromatin immunoprecipitation assays*

Antibody	Supplier	Product code	Source	WB	IP	ChIP
α-Smooth muscle	MilliporeSigma	A2547	Mouse	1:5000		
Actin (β)	MilliporeSigma	A5316	Mouse	1:20,000		
E-cadherin	BD Biosciences (San Jose, CA, USA)	610181	Mouse	1:1000		
EZH2	Cell Signaling Technology	5246	Rabbit	1:2000		1:100
Fibronectin	MilliporeSigma	F3649	Rabbit	1:5000		
H3	Abcam (Cambridge, MA, USA)	Ab1791	Rabbit	1:1000		
H3K27me3	Cell Signaling Technology	9733	Rabbit	1:1000		
Nanog	Abcam	ab21624	Rabbit	1:1000		
Oct4	Abcam	ab19857	Rabbit	1:1000		
Phospho- Smad3	Abcam	ab52903	Rabbit	1:1000		
Smad3	Abcam	ab28379	Rabbit	1:1000	4 μg	1 μg

ChIP, chromatin immunoprecipitation; IP, immunoprecipitation; phosphor, phosphorylated; WB, Western blot.

HEPES pH 7.5, 0.2 mM EDTA pH 7.4, 1.5 mM $MgCl_2$, 125 mM KCl, and 20% glycerol. Beads were incubated with nuclear lysates overnight at 4°C rotating with the addition of 250 U/ml of benzonase nuclease (Thermo Fisher Scientific). After overnight incubation, the beads were washed 5 times for 5 min in Buffer B with 0.02% NP-40 and 1 time for 5 min in Buffer B with no detergent. Immune complexes were eluted by boiling in 2× SDS sample buffer containing β-mercapoethanol at 95°C, or beads were prepared for mass spectrometry analysis as outlined below.

Immunoprecipitation of Flag-tagged proteins

Immunoprecipitation of Flag-tagged proteins was performed on whole cell extracts transfected with Flag-tagged Smad3 or an empty vector control and treated with TGF-β. Briefly, cells were lysed in 1 ml of RIPA supplemented with protease and phosphatase inhibitor cocktails as outlined above. One milligram of whole cell extract was immunoprecipitated with 40 μl of anti-Flag M2 affinity gel (MilliporeSigma) overnight at 4°C. Samples were spun at 5000 *g* for 30 s to pellet affinity gel, the supernatant was discarded, and the gel was washed 3 times with 500 μl of PBS. Immune complexes were eluted by boiling in 2× SDS sample buffer at 95°C for 3 min. One microliter of β-mercapoethanol was added to each sample, and samples were boiled again for 3 min to denature proteins. Samples were subject to Western blot analysis as previously outlined.

Isolation of histones and preparation for mass spectrometry

Histones were isolated according to the acid extraction method of Shechter *et al.* (19). Acid-extracted histones were then chemically acetylated with deuterated acetic anhydride (20) and quantified using the mass spectrometry MS1 ion current as described by Feller *et al.* (21). The resulting histone solution was subject to in-solution trypsin digestion prepared for mass spectrometry analysis.

In-solution trypsin digestion and mass spectrometry analysis

Samples were treated with trypsin and prepared for mass spectrometry as previously described (22) with some modifications. Briefly, C18 ziptips were used to bind peptides in solution instead of stage tips. Peptide samples were run on a Q Exactive Mass Spectrometer (Thermo Fisher Scientific) as previously described (17).

Data analysis

Mass spectrometry data were processed using MaxQuant software v.1.3.0.547 (23) using the human Uniprot database (release 2013_12). Perseus software was used to carry out statistical analysis (*http://www.perseus-framework.org*). Briefly, the intensity-based absolute quantification (iBAQ) values were transformed (log_2), and missing values were imputed to a normal distribution. Results were cleaned for reverse and contaminants, and a 2-tailed Student's *t* test was applied with correction for multiple testing using a false discovery rate of 0.01 to generate a list of significant interactors.

Immunofluorescence staining

Cells were fixed with 4% paraformaldehyde (Electron Microscopy Sciences, Hatfield, PA, USA) for 10 min, permeabilized with 0.1% Triton X-100 (MilliporeSigma) for 10 min, and blocked with 5% goat serum in PBS (MilliporeSigma) for 1 h at room temperature. Cells were stained with rhodamine phalloidin diluted in PBS for 30 min to visualize the F-actin filaments (1:500) (Thermo Fisher Scientific) and counterstained with Hoechst 33342 (1:1000) (Thermo Fisher Scientific) for 2 min to visualize the nucleus.

Quantitative PCR

Total RNA was isolated using Trizol reagent according to the manufacturer's instructions (Thermo Fisher Scientific). Five hundred nanograms of RNA was reverse transcribed to cDNA using the High Capacity cDNA Reverse Transcription Kit (Thermo Fisher Scientific) according to the manufacturer's instructions. Quantitative real-time PCR was performed using Taqman assays for E-cadherin, SNAI1, and Sybr Green primers for Smad3, EZH2, HOXA3, OCT4, and NANOG, as outlined in **Table 3**. PCR data were normalized to the endogenous controls glyceraldehyde-3-phosphate dehydrogenase (GAPDH) or RPO, respectively.

E-cadherin luciferase assay

ARPE19 cells were seeded into a 24-well tissue culture plate at a density of 75×10^3 cells per well. Cells were transfected in serum-free medium with the luciferase-containing construct (proE-cad670-Luc) and pCMVHA EZH2, pRK5F-Smad3, or both together, using Fugene HD transfection reagent (Promega). A plasmid encoding a constituently active thymidine kinase *Renilla* construct was cotransfected into all wells to control for transfection efficiency. Forty-eight hours after transfection, the cells were harvested in passive lysis buffer, and dual luciferase activity was measured using a Dual Luciferase Kit (Promega) according to the manufacturer's instructions. Firefly luciferase activity was normalized to *Renilla* values.

TGF-β secreted alkaline phosphatase assay

HEK Blue TGF-β reporter cells (InvivoGen, San Diego, CA, USA) were maintained according to the manufacturer's instructions.

TABLE 3. *Primer sequences for real-time PCR*

Gene	Primer sequence, 5′–3′	
	Forward	Reverse
Nanog	ATCTGCTTATTCAGGACAGCCC	GAAGTGGGTTGTTTGCCTTTG
OCT4	AAGAACATGTGTAAGCTGCGGC	CATTGTTGTCAGCTTCCTCCAC
EZH2	AGCTACATGTGAACCCACGGC	TTCTTGGAAGCTGCATAGTCACATAC
SMAD3	CAGTGGAGCTGACACGGAGAC	TCCCCTCCGATGTAGTAGAGCC
HOXA3	GGTTGCTGGAATGGCTGTAT	CCAAGAACCCTTCTGAACCA
RPO	TTCATTGTGGGAGCAGAC	CAGCAGTTTCTCCAGAGC

Primer sequences denote target gene only.

The cells were seeded into 24-well plates. Twenty-four hours after seeding, cells were serum restricted for 24 h followed by pretreatment with DZnep for 1 h. TGF-β was then added for 24 h. Ten microliters of sample supernatant was removed and added to 100 μl of Quanti-Blue secreted alkaline phosphatase detection mediuim in a 96-well plate and incubated at 37°C for 90 min. The absorbance was read at 620 nm on a Spectramax M2 Plate Reader (Molecular Devices, Sunnyvale, CA, USA).

Chromatin immunoprecipitation

ARPE19 cells were cultured and differentiated with TGF-β as previously outlined. Cells were fixed by addition of formaldehyde (Electron Microscopy Sciences; 16%) at a final concentration of 1% for 10 min to cross-link the cells. Fixation was quenched by the addition of 2 M glycine (final concentration, 0.125 mM) for 5 min. The cells were pelleted and lysed with cell lysis buffer containing 10 mM Tris-HCl pH 8.0, 10 mM NaCl, 0.2% NP-40, and 10 mM sodium butyrate with the addition of protease inhibitor cocktail. After centrifugation at 2500 rpm for 5 min, the pelleted nuclei were resuspended in an SDS buffer containing 50 mM Tris-HCl pH 8.1, 10 mM EDTA, 1% SDS, and 10 mM sodium butyrate with the addition of protease inhibitor cocktail. Samples were diluted in immunoprecipitation dilution buffer containing 20 mM Tris-HCl pH 8.1, 150 mM NaCl, 2 mM EDTA, 1% Triton X-100, 0.01% SDS, and 10 mM sodium butyrate with protease inhibitor cocktail followed by sonication using the Bioruptor (Diagnode, Seraing, Belgium). Chromatin samples were precleared for 1 h at 4°C using normal rabbit IgG. The sheared chromatin was precipitated overnight at 4°C using antibodies directed toward Smad3 or EZH2 with an isotype-matched control IgG (MilliporeSigma). The immune complexes were collected using protein G agarose beads (Roche, Basel, Switzerland), washed twice with a buffer containing 20 mM Tris-HCL pH 8.1, 50 mM NaCl, 2 mM EDTA, 1% Triton-x100, and 0.1% SDS, and then washed with a buffer containing 10 mM Tris-HCL pH 8.1, 250 mM LiCl, 1 mM EDTA, 1% NP-40, and 1% deoxycholic acid. Imuuune complexes were eluted by addition of an elution buffer containing 100 mM $NaHCO_3$, and 1% SDS for 15 min, shaking at 300 rpm. The cross-links were reversed, and DNA was extracted using phenol-chloroform according to standard procedures. Fifty nanograms of DNA was subject to standard PCR using previously published primers specific to the E-cadherin promoter region (24). Primers were as follows: forward, 5′-TAGAGGGTCACCGCGTCTAT-3′; reverse, 5′-TCACAGGTGCTTTGCAGTTC-3′. PCR amplification was carried out using Go Taq PCR Kit (Promega) according to the manufacturer's instructions. Cycling conditions were as follows: 1 cycle at 95°C for 9 min, 36 cycles consisting of 94°C for 1 min, 60°C for 1 min, and 1 cycle at 60°C for 10 min. The amplified fragments were separated on a 3% agarose gel and visualized with ethidium bromide.

RESULTS

Smad3 and EZH2 associate during differentiation of neuroepithelial NT2 cells

The TGF-β signaling pathway is recognized to play a role in early neural development (25). The role of Smad3 in this process has recently been demonstrated to be dependent on its nuclear distribution in a manner somewhat independent of TGF-β (26). Notably, Smad3 bound the promotors of many key developmental and specification genes that were also enriched for H3K27 trimethylation and H3K4 trimethylation bivalent histone marks, suggesting that both Smad3 and the polycomb repressive complex play key regulatory roles in self-renewal and differentiation networks in neural cells. To determine if Smad3 and PRC2 associate during neural specification, PRC2 was immunoprecipitated *via* the EZH2 subunit from nuclear extracts of NT2 cells during differentiation with retinoic acid. Extracts were trypsinized, and resulting peptides were identified and quantified using Orbitrap mass spectrometry, generating an EZH2 interactome. Components of the core complex (EZH2, SUZ12, and EED) were identified in both undifferentiated and differentiated cells, whereas a number of known PRC2-interacting proteins (MTF2, AEBP2, RBBP4 and 7, EZH1, PHF19, and PHF1) were unchanged during differentiation (**Fig. 1*A*** and Supplemental Fig. S1). Intriguingly, a number of transcription factors were identified as late EZH2-interacting proteins, including Smad3 (Fig. 1*A* and Supplemental Fig. S1) (17), raising the possibility that cooperation between PRC2 and TGF-β signaling may regulate neuroretinal cell fate.

During the time course of differentiation of NT2 cells, there was an increase in levels of total Smad3 and Smad3 phosphorylation (Fig. 1*B*), and Smad3 mRNA levels were also increased (Fig. 1*D*). The differentiation marker HOXA3 was also increased, indicating successful differentiation of the cells (Fig. 1*D*), whereas master transcription factors that regulate stemness and are known to co-occupy the genome with Smad3 in ESCs (3) (Oct4, Nanog) were absent in the differentiated (d 8) state compared with the undifferentiated (d 0) state (Fig. 1*B, D*). Significantly, although the levels of EZH2, the enzymatic component of the PRC2 complex, remained generally constant during differentiation (Fig. 1*B*), there was a global increase in bulk H3K27me3 levels in differentiated cells at d 8 (Fig. 1*C*). Both Smad3 and EZH2 were found primarily in nuclear fractions with an increase in nuclear Smad3 in response to retinoic acid treatment (Fig. 1*E*), and the direct binding between Smad3 and EZH2 was confirmed by coimmunoprecipitation (Fig. 1*F*). These results demonstrate that retinoic acid–mediated differentiation of NT2 neuroepithelial progenitor cells is characterized by increased levels of Smad3 and increased Smad3 phosphorylation, as well as increased H3K27me3 levels, and that during this process Smad3 and EZH2 physically associate.

The repressive histone mark H3K27me3 is increased during dedifferentiation of retinal epithelial cells in response to TGF-β

During the initiation and progression of diabetic microvascular complications, retinal epithelial cells are accepted to undergo dedifferentiation in response to hyperglycemia. This induces a process of reprogramming, evoking gene expression profiles reminiscent of ontogenesis, in response to increased levels of TGF-β in the eye. We wondered if the PRC2-regulated processes observed during NT2 differentiation could be driven by TGF-β in the pathologically relevant context of epithelial-to-mesenchymal transdifferentiation of neuroretinal pigmented epithelial cells. ARPE19 cells were dedifferentiated by stimulation

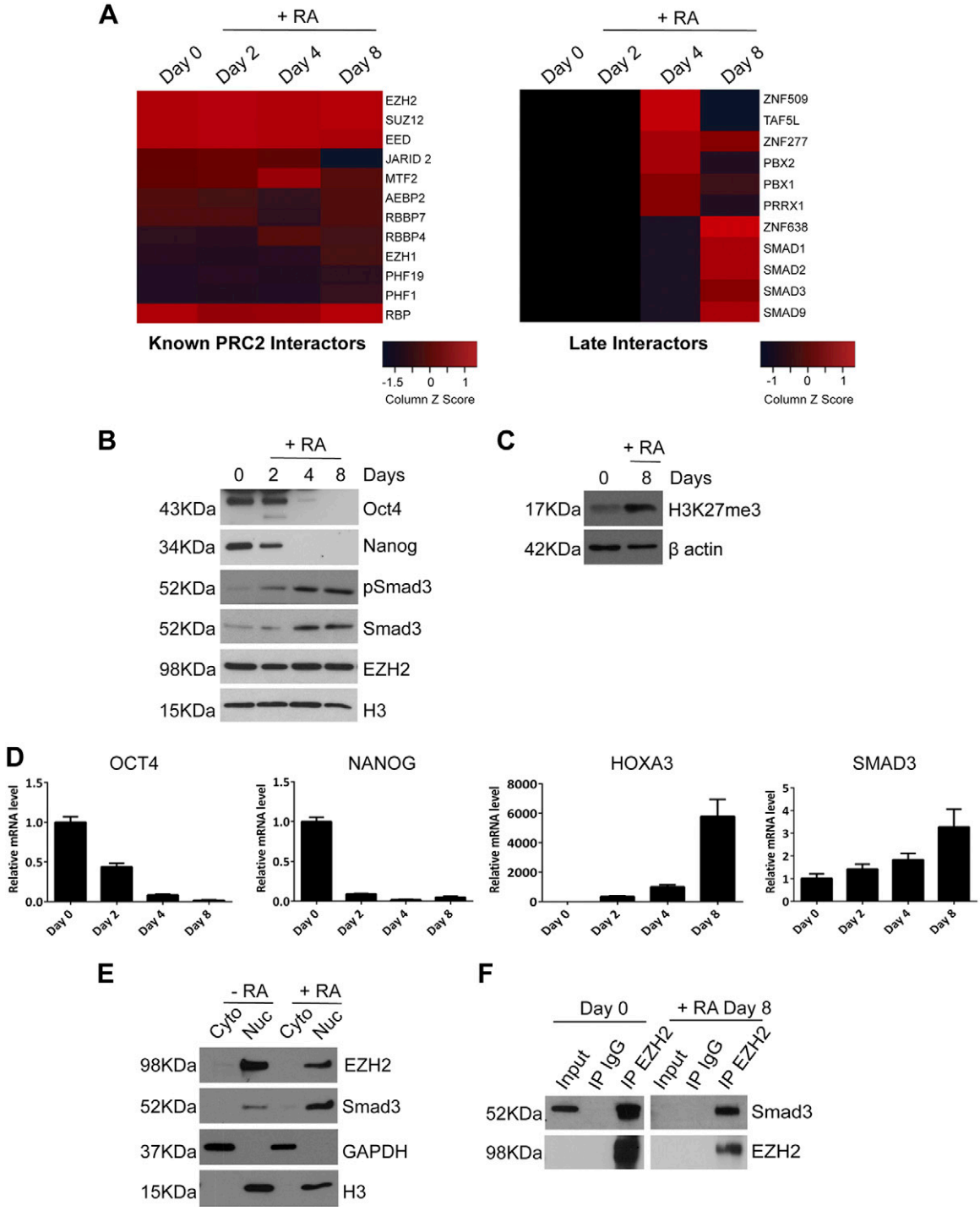

Figure 1. Smad3 was identified as a late EZH2 interactor during NT2 differentiation. *A*) Graphic representation of the EZH2 interactors identified by Orbitrap mass spectrometry in NT2 cells. The core PRC2 components EZH2, SUZ12, and EED, as well as a number of known PRC2 interactors (MTF2, AEBP2, RBBP4 and 7, EZH1, PHF19, PHF1), were identified as associated with EZH2 in undifferentiated and differentiated NT2 cells. The levels of JARID 2, a known PRC2 interactor, was decreased during NT2 differentiation with retinoic acid, and Smad3 was identified as a late PRC2-interacting protein. *B*) Western blot analysis of undifferentiated NT2 cells (d 0) and NT2 cells treated with retinoic acid to induce differentiation (d 2, 4, 8). H3 was used as a loading control. *C*) Western blot for the repressive histone mark H3K27me3. H3K27me3 expression was increased in differentiated cells treated with retinoic acid (d 8) compared with undifferentiated cells (d 0). *D*) Real-time PCR quantification of OCT4, NANOG, SMAD3, and HOXA3 in undifferentiated NT2 cells (d 0) and cells differentiated with retinoic acid (d 2, 4, 8). Expression levels of mRNA were normalized to RPO housekeeping gene. *E*) Nuclear (Nuc) and cytoplasmic (Cyto) fractionation of NT2 cells with and without retinoic acid. Lysates were subjected to Western blot analysis and probed for Smad3 and EZH2. GAPDH was used as cytoplasmic loading control, and H3 was used a nuclear loading control. *F*) Direct binding between Smad3 and EZH2 was confirmed by coimmunoprecipitation in undifferentiated and differentiated NT2 cells. IP, immunoprecipitation; RA, retinoic acid.

with TGF-β, and established markers of epithelial and mesenchymal fates were assessed by Western blot analysis. The epithelial marker E-cadherin was reduced after stimulation with TGF-β with parallel increases in the mesenchymal markers α smooth muscle actin and fibronectin (**Fig. 2*A***). Furthermore, cells also exhibited loss of cortical actin and *de novo* assembly of stress fibers suggestive of epithelial-to-mesenchymal dedifferentiation (Fig. 2*B*). Many of the profibrotic actions of TGF-β are mediated by Smad3, which is known to regulate the expression of a number of EMT-associated transcription factors including Snail (27). Both phosphorylated Smad3 and Snail were increased by TGF-β treatment (Fig. 1*A*). Stable repression of epithelial genes is required to facilitate phenotypic switches associated with EMT. Therefore, we hypothesized that chromatin modifications associated with gene repression and heterochromatin may be altered during EMT to enable such transitions. We examined bulk levels of the repressive histone mark H3K27me3 by Western blot analysis and observed an increase in levels of this histone modification during TGF-β–mediated epithelial-to-mesenchymal dedifferentiation (Fig. 1*A*). These findings were confirmed by quantitative mass spectrometry analysis of H3K27me3 levels (Supplemental Fig. S2); similarly, during NT2 differentiation, the levels of EZH2 (the methyltransferase responsible for catalyzing the formation of the mark) remained relatively constant. To confirm that increased H3K27me3 is a canonical, TGF-β and Smad3–driven event, we transfected ARPE19 cells with a full-length Flag-tagged Smad3–overexpression plasmid for 48 h in the absence of TGF-β. H3K27me3 expression was increased in cells transfected with Smad3 relative to nontransfected cells or empty vector controls. Successful overexpression was confirmed by probing for Flag tag (Fig. 2*C*). These results suggest that the processes observed during neuroepithelial NT2 differentiation, specifically increased phosphorylation of Smad3 and increased levels of H3K27me3, are paralleled during pathologically relevant TGF-β–driven dedifferentiation of ARPE19 epithelial cells.

Smad3 and EZH2 associate during dedifferentiation of neuroretinal epithelial cells in response to TGF-β

After our observation that H3K27me3 was also increased during TGF-β–mediated epithelial-to-mesenchymal dedifferentiation of retinal epithelial cells, we next asked if EZH2 and Smad3 also associate in this context. We confirmed that EZH2, Smad3, and phosphorylated Smad3 were localized to the nuclear compartment by subcellular fractionation (Fig. 2*D*). To map the EZH2 interactome, we performed endogenous immunoprecipitation with EZH2 and a matched IgG control in ARPE19 nuclear lysates dedifferentiated with TGF-β for 72 h followed by trypsin digestion, identification, and quantitation of peptides using Orbitrap mass spectrometry as previously described. EZH2 and the core components of the PRC2 complex (SUZ12 and EED) were immunoprecipitated under both experimental conditions (TGF-β *vs.* control), whereas

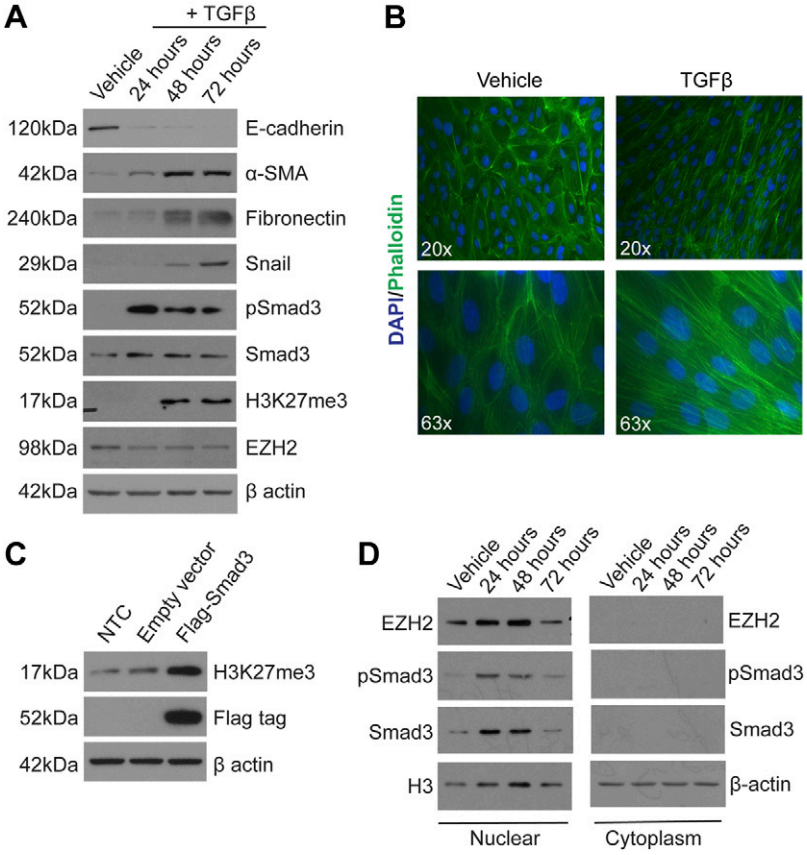

Figure 2. TGF-β induces dedifferentiation in ARPE19 cells, and during this process expression of the histone mark H3K27me3 is increased. *A*) ARPE19 cells were treated with recombinant human TGF-β for 24, 48, and 72 h. The expression of known markers of epithelial and mesenchymal fates, as well as the expression of the histone mark H3K27me3, were examined by Western blot. β-actin was used as a loading control. *B*) Immunofluorescent staining of F-actin fibers using phalloidin stain demonstrates loss of cortical actin and *de novo* assembly of stress fibers in response to TGF-β treatment. *C*) Flag-tagged Smad3 was overexpressed for 48 h in ARPE19 followed by Western blot analysis for the histone mark H3k27me3. Successful overexpression is indicated by expression of the Flag tag. *D*) Western blot of nuclear and cytoplasmic fractions of cells treated with vehicle or TGF-β. The expression of Smad3 and EZH2 was detected. GAPDH was used a cytoplasmic loading control, and H3 was used as a nuclear loading control. NTC, nontransfected control.

Smad3 was enriched in the TGF-β–treated cells compared with vehicle control (**Fig. 3*A***). The IgG control did not pull down EZH2 or any of the core PRC2 complex components, indicating the relative specificity of the antibody. Volcano plots were used to plot the enrichment of identified EZH2 interactors (relative to an IgG antibody control) against the significance of that fold enrichment. Representative volcano plots of the data from liquid chromatography with tandem mass spectrometry indicate peptides that interact with EZH2 (Fig. 3*B*). The bait protein (EZH2), core components of the PRC2 complex (SUZ12, EED), and a number of known accessory proteins (RBBP7, RBBP4, PHF1) were among the most significant scoring under both experimental conditions, as indicted by their relative fold change and *P* values. Smad3 scored insignificant under vehicle conditions; however, it was detected as a highly significant interactor under TGF-β–treated conditions (Fig. 3*B*). iBAQ scoring was used to determine the stoichiometry of PRC2 core components, accessory proteins, and novel interacting proteins relative to EZH2 using the method of Smits *et al.* (28). EZH2 interacts with EED in a 1:1 ratio and SUZ12 in a 1:1.5 ratio, in agreement with previously published data (Fig. 3*C*) (28). Smad3 was almost undetectable under control conditions but increased in response to TGF-β. Direct interaction between Smad3 and EZH2 in the chromatin-associated nuclear fractions was confirmed by coimmunoprecipitation analysis and reverse endogenous coimmunoprecipitation (Fig. 3*D, E*). Furthermore, this interaction was additionally confirmed in HEK293T cells overexpressing Flag-tagged Smad3 and treated with TGF-β. EZH2 copurified with Smad3 when the Flag tag was used to immunoprecipitate Smad3 (Fig. 3*F*). These results indicate that Smad3 and EZH2 also associate during TGF-β–mediated dedifferentiation of neuroretinal epithelial cells.

Targeting the Smad-EZH2 complex inhibits TGF-β–mediated epithelial dedifferentiation

Next, we asked if inhibiting either Smad3 or EZH2 could protect cells from undergoing TGF-β–mediated epithelial dedifferentiation. In our initial approach we used small molecule inhibitors of Smad3 activation and EZH2 activity. SB431542 is a potent TGF-β type I receptor inhibitor that inhibits the kinase activity of the type 1 receptor preventing activation of downstream Smad signaling (29). SB431542 effectively inhibited TGF-β–mediated phosphorylation of Smad3 in ARPE19 cells (**Fig. 4*A***). Pretreatment of cells with SB431542 protected against TGF-β–mediated loss of E-cadherin. Furthermore, SB431542 prevented the induction of the mesenchymal markers fibronectin, α-smooth muscle actin, and Snail (Fig. 4*A*). Treatment with the inhibitor did not affect levels of EZH2 (Supplemental Fig. S3). DZnep is an inhibitor of S-adenosylmethionine–dependent methyltransferases and has been shown to decrease the activity of EZH2 in cells (30). Pretreatment of cells with DZnep prevented TGF-β–mediated induction of both α smooth muscle actin and Snail; however, DZnep did not prevent the induction of fibronectin or the loss of E-cadherin (Fig. 4*B*). Furthermore, pretreatment with DZnep did not affect the phosphorylation of Smad3 or inhibit secreted alkaline phosphatase promotor reporter activity (Fig. 4*B* and Supplemental Fig. S3). Although pretreatment of cells with DZnep decreased the levels of EZH2 only marginally after 48 and 72 h, global levels of H3K27me3 were decreased by 24 h and further decreased by 48 and 72 h after treatment (Fig. 4*C*). However, DZnep is not a direct EZH2 inhibitor; instead, it inhibits S-adenosyl homocysteine hydrolase, which leads to degradation of the PRC2 complex *via* a feedback inhibition mechanism. DZnep is known to inhibit histone marks other than H3K27me3, including H4K20me3 (31). In order to establish that the effects of DZnep were not due to inhibition of other methyltransferases, we repeated the experiment with a more selective inhibitor of EZH2, GSK343. GSK343 is a *S*-adenosyl-L-methionine–competitive inhibitor, highly potent and selective for EZH2 (32). GSK343 inhibited EZH2 expression and decreased global levels of H3K27me3 after 48 h of treatment (Fig. 4*D*). Although pretreatment of cells with GSK343 prior to treatment with TGF-β prevented the induction of fibronectin, it did not protect against TGF-β–mediated loss of E-cadherin.

In a second approach, we used esiRNAs to knock down Smad3 and EZH2 for 48 h followed by treatment with TGF-β for 48 h. Successful knockdown was achieved for both Smad3 and EZH2 alone or in combination (Fig. 4*E*). Furthermore, Smad3 knockdown also inhibited phosphorylation of Smad3, whereas knockdown of EZH2 had no discernable effect. We examined the effect of Smad3 or EZH2 knockdown or double knockdown of Smad3 and EZH2 on fibronectin and E-cadherin expression. Smad3 knockdown reduced TGF-β–mediated fibronectin induction relative to scrambled control, whereas EZH2 knockdown had a minimal effect. Knockdown of both Smad3 and EZH2 completely inhibited this response (Fig. 4*F*). Although there was some loss of basal E-cadherin in response to Smad3 knockdown, EZH2 knockdown resulted in complete loss of E-cadherin protein expression, particularly in cells treated with TGF-β. Double knockdown of Smad3 and EZH2 partially restored basal levels of E-cadherin (Fig. 4*F*).

Smad 3 and EZH2 cooperate to regulate cellular plasticity in retinal epithelial cells

Having established that EZH2 and Smad3 associate with each other in multiple contexts (Figs. 1 and 2), we considered what the functional implications of this interaction might be. Two separate, striking pieces of information led us to speculate that the interaction between Smad3 and EZH2 might direct the PRC2 complex to specific loci and is generally repressive in nature. Firstly, we observed an inverse relationship between the expression of the pluripotency factors (Oct, Sox, Nanog) and Smad3 and EZH2 during the course of NT2 differentiation (Fig. 1*B, D*). Secondly, analysis of available chromatin immunoprecipitation sequencing (ChIP-seq) data from the

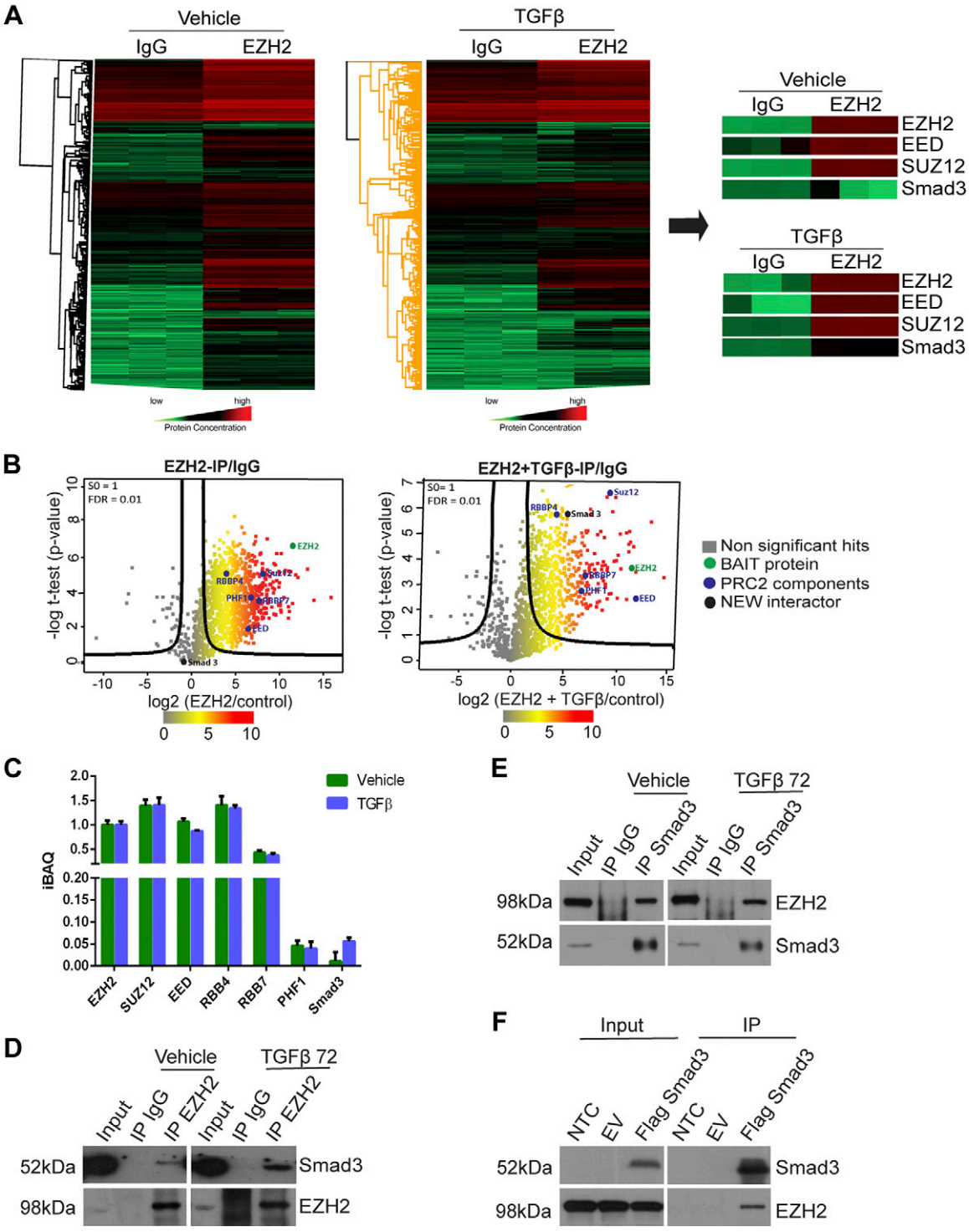

Figure 3. Proteomic analysis of the EZH2 interactome during TGF-β–mediated epithelial dedifferentiation in ARPE19 cells identifies an interaction with Smad3. Endogenous immunoprecipitation with EZH2 in ARPE19 cells dedifferentiated with TGF-β for up to 72 h was followed by trypsin digestion, identification, and quantitation of peptides using Orbitrap mass spectrometry. *A*) Heat map indicating the differential abundances of proteins in vehicle *vs.* TGF-β–treated cells. *B*) Volcano plots of data from liquid chromatography with tandem mass spectrometry for vehicle and TGF-β conditions. Differences in Student's *t* test scores between specific and control immunoprecipitation were plotted against log-transformed Student's *t* test *P* values with a false discovery rate (FDR) set to 0.01. The bait protein EZH2 (BAIT) is labeled in green. The components of the PRC2 complex are labeled in blue, and newly identified interactors (NEW) are labeled in black. S0, artificial within groups variance. *C*) iBAQ values were scaled to the bait protein for each condition to plot relative stoichiometry data for core and previously described PRC2 components, as well as for the newly identified interactor Smad3. *D, E*) Direct binding between Smad3 and EZH2 was confirmed by EZH2 coimmunoprecipitation and Smad3 reverse coimmunoprecipitation. *F*) HEK293 cells were transfected with a wild-type Flag-tagged Smad3 followed by treatment with TGF-β for 48 h. Smad3 was immunoprecipitated from a whole-cell lysate using anti-Flag affinity gel, and EZH2 was detected by Western blot. EV, empty vector; IP, immunoprecipitation; NTC, nontransfected control.

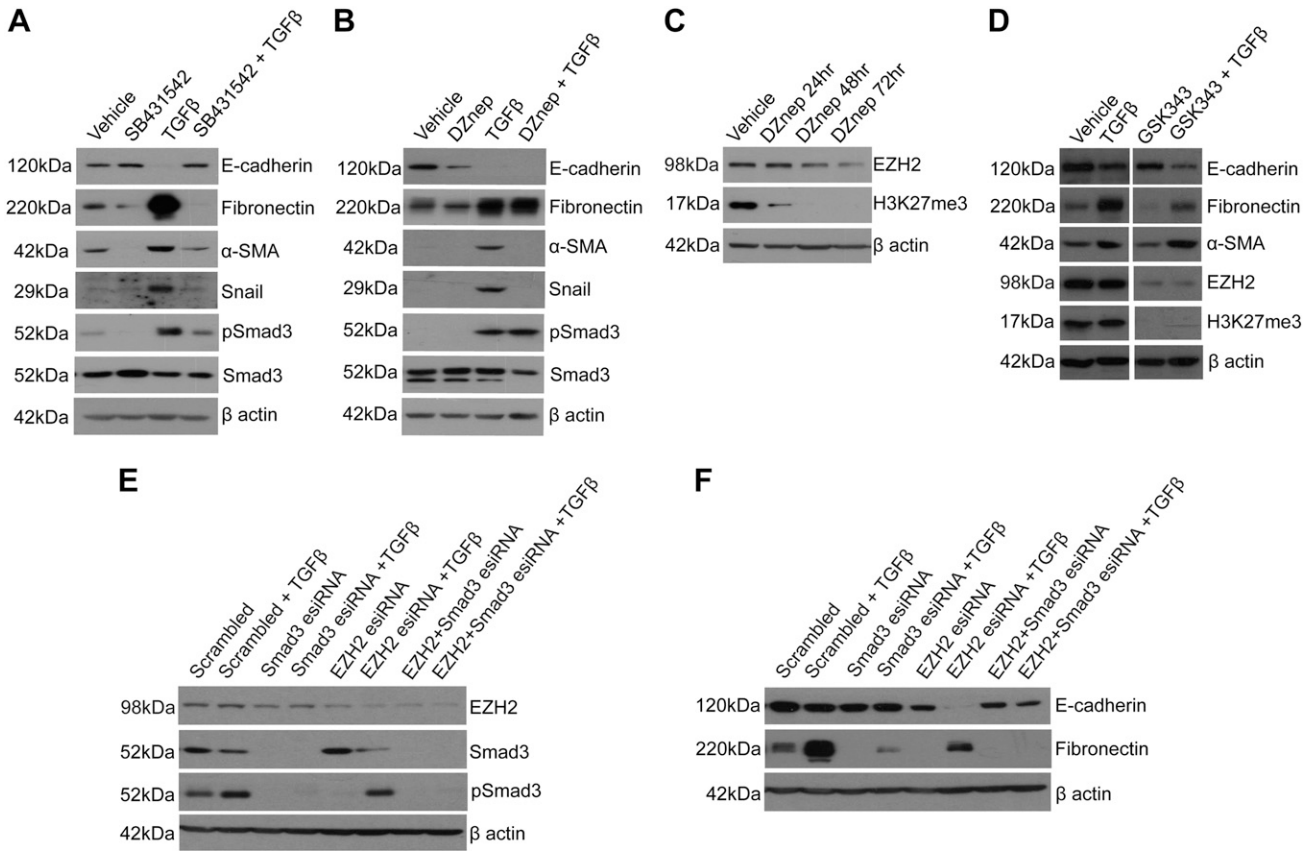

Figure 4. Targeting the Smad-EZH2 complex using small molecule inhibitors and esiRNA knockdown. *A*, *B*) Pharmacological inhibition of the TGF-β type I receptor and EZH2 using the small molecule inhibitors SB431542 (10 μM) and DZnep (5 μM), respectively. Cells were pretreated for 1 h with the inhibitor prior to treatment with TGF-β for 48 h. *C*) DZnep treatment of ARPE19 cells resulted in decreased EZH2 expression at 48 and 72 h after treatment, and repressive chromatin mark H3K27me3 was decreased by 24 h and further reduced at 48 and 72 h after treatment. *D*) Pharmacological inhibition of EZH2 using the more specific inhibitor, GSK343. Cells were pretreated for 1 h with the inhibitor (5 μM) prior to treatment with TGF-β followed by Western blot analysis of epithelial and mesenchymal markers. *E*) Smad3 and EZH2 were knocked down individually or in combination using esiRNA technology. Knockdown was confirmed by Western blot analysis. Smad3 knockdown also inhibited the phosphorylation of Smad3, whereas EZH2 knockdown had no effect. *F*) Effect of knockdown of Smad3 and EZH2 on epithelial and mesenchymal (E-cadherin and fibronectin) markers in the presence and absence of TGF-β was assessed by Western blot.

ENCODE project revealed the presence of bivalent trimethyl marks (H3K4Me3 and H3K27Me3) at the CDH1 gene locus in NT2 cells, whereas in ESCs, the repressive mark is absent, suggesting the resolution of a monovalent, transcriptionally permissive state to the bivalent state during differentiation (**Fig. 5*A***). Similarly, the repressive mark is not present in epithelial cells characterized by high levels of E-cadherin, whereas in myofibroblasts there is increased H3K27Me3 (Fig. 2*A*). Further interrogation of the Mullen ChIP-seq data set revealed 267 bivalent loci that are Smad3 bound in human ESCs and a further 438 that are silenced (Fig. 5*B*). Intriguingly, silenced Smad3-bound loci were significantly enriched for cell adhesion molecules, including several cadherins and protocadherins. Gene ontology analysis using Panther revealed significant enrichment of developmental and morphogenic processes among bivalent Smad3 bound genes, of which 36.6% are classified as transcription factors (Fig. 5*C*). These include a number of transcription factors that are implicated in cell fate specification and development. Each of the 61 transcription factors was subsequently interrogated using existing ChIP-seq data from the ENCODE project. All Smad3-bound loci are additionally EZH2 bound. Comparative analysis using chromatin immunoprecipitation correlation identified a number of highly enriched EZH2 features (8–27-fold enrichment) typically within 1000 bp of Smad3 bound site.

In adult cells, during EMT, it has been proposed that Smad3 in complex with Smad4 recruits Snail to the E-cadherin promoter to repress its expression (33). Additionally, the recruitment of PRC2 to the E-cadherin promoter by Snail has been demonstrated in cancer cells and during embryonic development (24, 34–36); however, a link between these 2 observations has remained elusive, and to date few studies have addressed the mechanism through which Smad3 can regulate plasticity by controlling promoter accessibility of key epithelial genes. We hypothesized that the

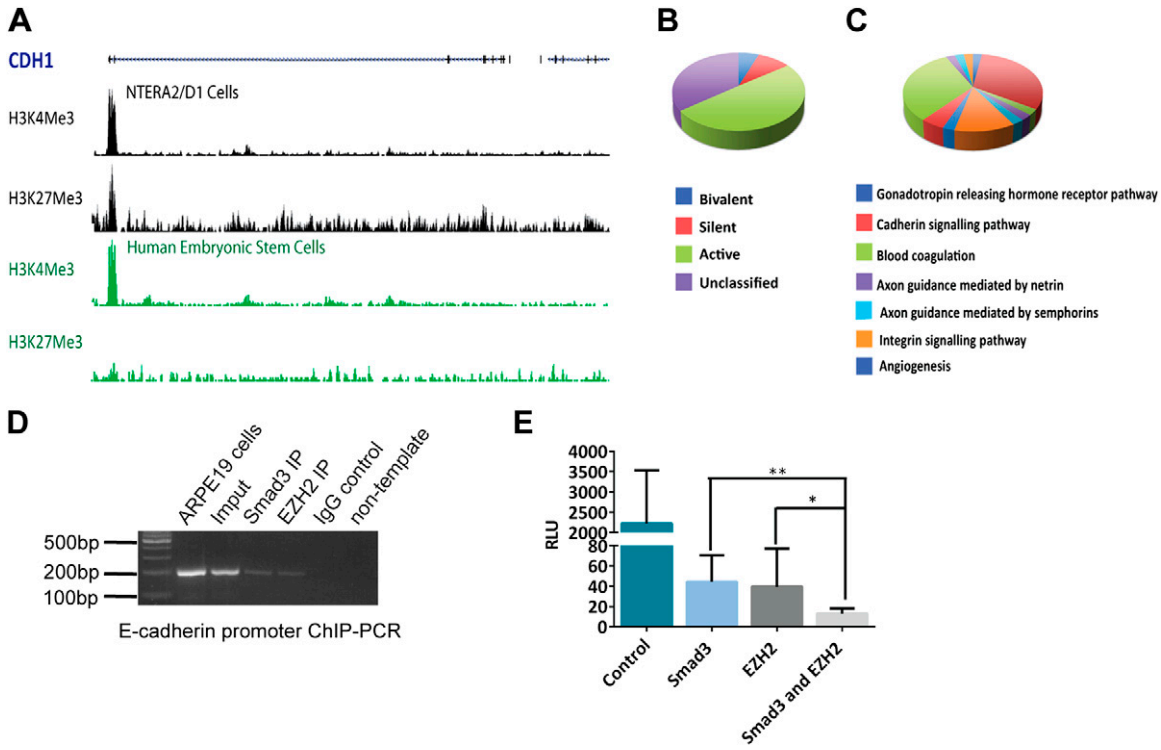

Figure 5. Smad3 and EZH2 cooperate to repress E-cadherin promoter-reporter activity. *A*) Genome Browser view of the E-cadherin (cdh1) locus illustrating H3K27me3 and H3K4me3 ChIP-seq tracks in ESCs and NT2 cells. *B*) Analysis of the Mullen ChIP-seq data classifying all Smad3-bound promotors in human ESCs as silent, bivalent, active, or unclassified. *C*) Gene ontology analysis of Smad3-silenced genes from the Mullen ChIP-seq data set. *D*) Chromatin immunoprecipitation–PCR (ChIP-PCR) analysis of the E-cadherin promoter for Smad3 and EZH2 occupancy in ARPE19 cells treated with TGF-β. The primers were designed to flank the promoter region of CDH1. A nontemplate sample as well as an isotype-matched control IgG served as negative controls, and DNA isolated from ARPE19 cells not subjected to chromatin shearing or immunoprecipitation (IP) and an input sample subjected to chromatin shearing but not immunoprecipitation served as positive controls. *E*) Overexpression of both Smad3 and EZH2 individually reduce E-cadherin luciferase activity in ARPE19 cells, with the greatest reduction in luciferase activity observed with both in combination. RLU, Relative Luciferase Unites. $^{*}P < 0.05$, $^{**}P < 0.01$.

interaction of Smad3 and EZH2 might function to recruit the PRC2 complex to the E-cadherin promoter and silence its expression. We first established co-occupancy of Smad3 and EZH2 on the CDH1 proximal promoter under differentiation conditions by chromatin immunoprecipitation followed by PCR (Fig. 5*D*). Briefly, ARPE19 cells were dedifferentiated with TGF-β for 48 h. Chromatin fractions were immunoprecipitated using antibodies against Smad3 and EZH2 followed by amplification of the E-cadherin proximal promoter using previously published primers (24). Both Smad3 and EZH2 were present on the promoter under these conditions. In order to test if Smad3 and EZH2 co-occupancy facilitated repression of CDH1, we utilized a promoter reporter construct comprising a 670 bp region of the CDH1 promoter upstream of the transcription start site. We determined that although overexpression of either Smad3 or EZH2 significantly repressed reporter activity, there was a clear synergistic response when both EZH2 and Smad3 were co-overexpressed (Fig. 5*E*). These results suggest that Smad3 and EZH2 occupy the E-cadherin promotor during TGF-β–mediated dedifferentiation and suggest these factor may cooperate to repress E-cadherin expression.

Inhibition of Smad3 signaling using a TGF-β receptor targeting microRNA rescues expression of E-cadherin

The miR302/367 cluster was initially identified as a potential stemness regulator in ESCs (37). We subsequently identified the TGF-β type II receptor as a target of miR302 and demonstrated ablation of Smad3 signaling and the acquisition of plasticity in adult cells overexpressing miR302 (14, 16). We hypothesized that silencing of the TGF-β type II receptor with miR302 could be used to perturb the interaction between Smad3 and EZH2. A polycistronic plasmid encoding all 4 members of the miR302 family was used to generate a miR302 lentivirus. Lentiviral overexpression of miR302 in ARPE19 cells resulted in significantly increased expression of E-cadherin at both protein and mRNA level (**Fig. 6*A, B***) compared with both nontransduced and scrambled controls. Intriguingly, this was initially associated with increased Snail and EZH2 (d 7), resolving to a state of high levels of E-cadherin, concomitant with loss of Snail and EZH2 (d 14) (Fig. 6*A, B*). Even in the presence of TGF-β, miR302 overexpression facilitated increased E-cadherin expression and dampened TGF-β–induced α smooth muscle actin expression, protecting the cells from

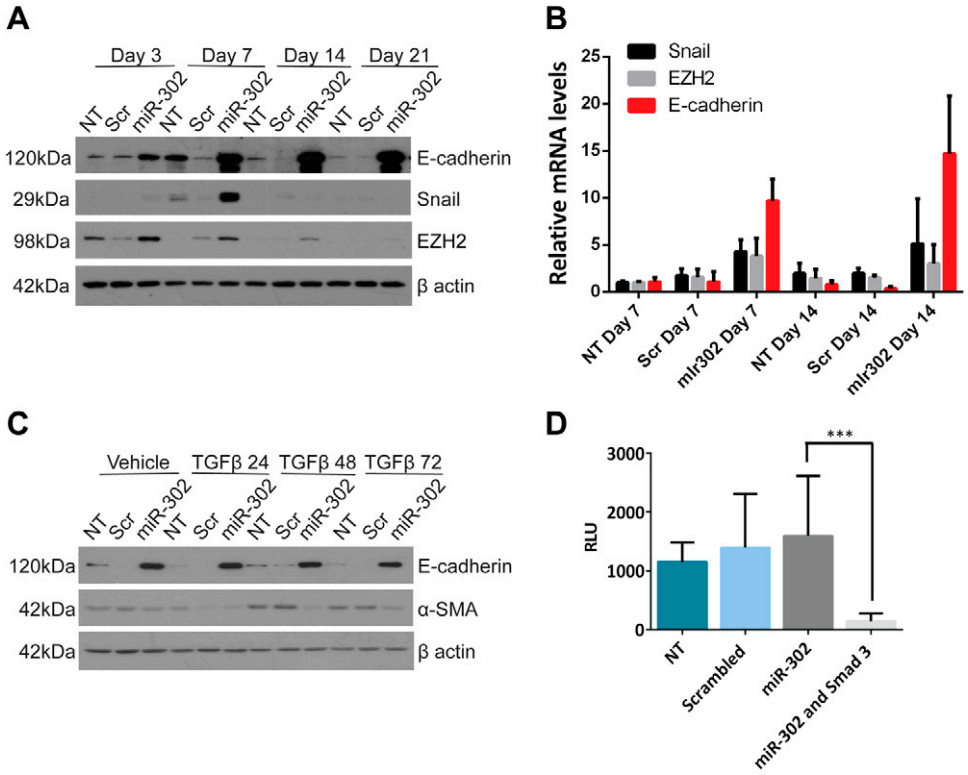

Figure 6. miR302 increases the expression of E-cadherin. *A*) Lentiviral overexpression of miR302 in ARPE19 cells increased the expression of E-cadherin, EZH2, and Snail compared with nontransduced and scrambled controls. *B*) Real-time PCR quantification of increased E-cadherin, EZH2, and Snail in response to miR302. *C*) Western blot analysis of E-cadherin and α smooth muscle actin in ARPE19 nontransduced cells or in cells transduced with miR302 or a scrambled control virus for 7 d followed by treatment with TGF-β or a vehicle control for 24, 48, or 72 h. *D*) Analysis of E-cadherin luciferase activity in miR302-overexpressing cells with or without transient overexpression of Smad3. Briefly, ARPE19 cells were transduced with miR302 lentivirus or a control scrambled virus or left nontransduced for 7 d. At d 7, cells were reseeded and transfected with an E-cadherin luciferase construct and a *Renilla* internal control with or without a Smad3 expression vector for 48 h. RLU, Relative Luciferase Units. ***$P < 0.001$. NT, nontransduced; Scr, scrambled.

undergoing TGF-β–mediated dedifferentiation (Fig. 6*C*). Furthermore, overexpression of miR302 had no discernable effect on E-cadherin promoter reporter activity at d 7 after transduction despite increased levels of EZH2 and Snail, whereas transient overexpression of Smad3 in these cells led to almost complete inhibition of E-cadherin promoter reporter activity (Fig. 6*D*).

DISCUSSION

Here we demonstrate a physical interaction between EZH2, the enzymatic core of the PRC2 complex, and Smad3 during retinoic acid–mediated differentiation of neuroepithelial pluripotent NT2 cells and the dedifferentiation of neuroretinal epithelial ARPE19 cells in response to TGF-β and elaborate on the functionality of this interaction.

Researchers have struggled to explain how cells interpret TGF-β signaling in pluripotent *vs.* differentiating conditions, more specifically the role of Smad2 and -3 in the resolution of poised bivalent to monovalent states, either repressive or permissive, during specification. Baker *et al*. in Stanford first proposed a mechanism whereby SMAD proteins coordinate with chromatin at critical promoters during endodermal specification (38). Subsequent studies identified HEB and E2A as Smad3 cofactors and demonstrated that HEB directly associates with PRC2 at a subset of developmental promoters in a nodal-independent manner, whereas its association with Smad2 and -3 is nodal dependent. A simple interpretation of this data would suggest that Smad3, HEB, and PRC2 form a dynamic complex during endoderm specification (39). Similarly, we identified an association between Smad3 and the enzymatic core of the PRC2 complex, EZH2, which was enriched during the differentiation of neuroepithelial NT2 cells. Our group previously mapped PRC2 interactors in undifferentiated NT2 *vs.* differentiated NT2 cells, noting dynamic changes to the PRC2 interactome between cell states, namely, a shift from association with factors known to be involved in stemness, such as SALL4 and ZNF281, to association with factors with recognized roles in processes related to differentiation, such as Smad3 and PLC1 (40). Smad3 transcript and protein levels, as well as Smad3 phosphorylation, were increased during retinoic acid–mediated NT2 differentiation, inversely correlating with the levels of the master transcription factors Oct4 and Nanog, known to regulate stemness, suggesting that Smad3 signaling may play an important role in directing the neural differentiation program. In fact, Smad3 was previously shown to facilitate neural differentiation by promoting the switching of neural progenitor cells to neural precursors (25).

Importantly, the dynamic changes to the PRC2 interactome were accompanied by increases in the H3K27me3 histone mark at d 8, leading us to hypothesize that the regulation of neuroepithelial cell fate thus involves carefully choreographed chromatin reorganization controlled by the interaction between Smad3 and EZH2.

Critically, we also demonstrated an association between Smad3 and EZH2 in response to TGF-β–mediated EMT, highlighting the widespread nature of this complex.

The association between the 2 factors was enriched under TGF-β treated conditions relative to control and, as during NT2 differentiation, correlating with increased levels of H3K27me3. Importantly, Smad3 and EZH2 form a complex that is directed to the CDH1 locus and is repressive in nature. Smad3-driven recruitment of Snail1 to the E-cadherin promotor to facilitate repression is well established during EMT (33, 41). Furthermore, the recruitment of PRC2 to the E-cadherin promoter by Snail1 has been demonstrated in numerous contexts, including cancer cells and differentiating ESCs (34, 36, 42). Interestingly, a recent study mapped the binding kinetics of Snail1 to its target promoters during EMT. The researchers observed transient binding of Snail1 to the E-cadherin promotor, which peaked at 6 h after EMT induction and preceded deposition of the repressive H3K27me3 histone mark (43). Accumulation of H3K27me3 suggests PRC2-mediated stable silencing of gene expression. Consistent with this, we demonstrated occupancy of the E-cadherin promotor by Smad3 and EZH2 48 h after TGF-β treatment, coincident with the appearance of the H3K27me3 histone mark. Although binding of Snail1 to its target promotors, including E-cadherin during EMT, may represent an initiating silencing event, long-term repression is likely mediated by a mechanism independent of Snail1 binding. Indeed, displacement of Snail1 from the promotor may enable stable silencing by facilitating the formation of the Smad3-EZH2 repressive complex and promote deposition of H3K27me3 to regulate alterations in the chromatin landscape. However, further investigation is warranted to confirm this hypothesis.

In the context of our cell model, manipulation of this complex using pharmacological inhibitors of Smad3 and EZH2 activity facilitated the reassembly of adherens junctions and the rescue of epithelial phenotype in the case of SB431542 but not in the case of either of the EZH2 inhibitors. Similarly, knockdown of EZH2 failed to rescue E-cadherin expression. A simple interpretation of this data would suggest that inhibiting Smad3 phosphorylation is critical to prevent repression of E-cadherin and that although DZnep and EZH2 esiRNA knockdown inhibited EZH2 activity and expression, respectively, neither affected Smad3 phosphorylation; thus Smad3 may still be recruited to the E-cadherin promotor to facilitate repression in a PRC2-independent mechanism. In an alternative strategy, we disrupted Smad3 signaling by overexpressing miR302. Our laboratory, among others, has previously validated the TGF-β type II receptor as a miR302 target (14, 44). Mechanistically, miR302 downregulates the expression of TGF-β type II receptor; consequently, phosphorylation of Smad3 is blocked. Intriguingly, overexpression of miR302 not only maintained E-cadherin expression but in fact increased basal levels of E-cadherin at both a transcript and a protein level despite increased levels of both Snail1 and EZH2. This induction of E-cadherin in response to miR302 overexpression was not ablated by treatment with TGF-β, further suggesting that functional Smad3 signaling is required for polycomb-mediated repression of E-cadherin in response to TGF-β. At d 7, when cells exhibited the highest expression of both Snail1 and EZH2, E-cadherin promoter-reporter activity was unaffected in miR302-overexpressing cells relative to control, whereas transient overexpression of Smad3 was sufficient to repress this activity. Similarly, in another study from our group, we demonstrated that overexpression of miR302 also increases levels of EZH2 and Snail1 in human mesangial cells during acquired plasticity (16). Overexpression of miR302 in combination with treatment with DZnep resulted in *de novo* expression of E-cadherin in these cells, which, being of fibroblast origin, do not express E-cadherin endogenously. Although the precise mechanism of this *de novo* expression of E-cadherin was unclear at the time, it seems plausible in the light of the data presented in this study that miR302 *via* modulation of Smad signaling disrupts the association between Smad3 and EZH2, leading to loss of stable repression of the E-cadherin promoter. miR302 expression alone was sufficient to increase basal levels of E-cadherin expression in epithelial cells, whereas in fibroblasts, overexpression of miR302 required the addition of DZnep to achieve the same result, likely reflecting the permissive state of the CDH1 promotor in epithelial cells, which is subsequently resolved to a monovalent polycomb stably repressed state in fibroblasts.

Likewise, in pluripotent cells, such as human and mouse ESCs, a large subclass of enhancers are marked by H3K27me3 and bound by the polycomb complex PRC2 (45, 46). These elements have been termed "poised enhancers" and are located near key early developmental genes yet are unable to drive gene expression in pluripotent cells—an ability they acquire during differentiation, coincident with the loss of H3K27me3. Consistently, genes located in proximity of H3K27-methylated enhancers commonly have so-called bivalently marked promoters, characterized by the simultaneous presence of H3K4me3 and H3K27me3 and association with PRC2. H3K27me3 enrichment has not been widely described at enhancers in other differentiated cell types, suggesting that poised enhancers in ESCs may reflect unique polycomb regulation in pluripotent cells. However, given the shared characteristics between stem and progenitor populations undergoing differentiation and cells during the acquisition of plasticity associated with transdifferentiation and pathologic cell dedifferentiation, this raises the intriguing possibility that a similar mechanism is employed. In light of the fact that Smad3 and EZH2 association was enriched under both NT2 cell differentiation and TGF-β–mediated dedifferentiation, it is tempting to suggest that this may represent a general mechanism through which Smad3 directs repression of genes; however, clearly more investigation is required. Notably, Smad3 was found to be associated with the other core components of the PRC2 complex in studies by our group and others. Smad3 associates with Suz12 during NT2 differentiation (17). EED was found to associate with Smad3 in neural progenitor cells but not ESCs (47), further suggesting that interactions between Smad3 and the PRC2 complex directs its activity during fate transitions. However, it must be noted that the current study was undertaken using immortalized cell lines. Although ARPE19 cells are not an exact model of retinal pigmented epithelial cells *in vivo*, they have many

properties similar to primary retinal pigment epithelium that make them a useful model, including an intact TGF-β signaling pathway. However, additional studies in primary cells are warranted to confirm the observations presented in this manuscript. We have recently derived retinal pigmented epithelial cells from induced pluripotent stem cells, and these cells dedifferentiate in response to TGF-β in a manner similar to ARPE19 cells (unpublished results). Nevertheless, our integrated signaling and proteomic approach to dynamically map the polycomb repressive complex during cell differentiation provide important insights into the cooperative nature of the interaction between the transcriptional machinery responsible for establishing specified states and the epigenetic mechanisms that facilitate these transitions. FJ

ACKNOWLEDGMENTS

The authors acknowledge the help of the University College Dublin (UCD) Conway Genomics and Proteomics Core Facilities. The authors also acknowledge Dr. Adrian Bracken (Trinity College Dublin), for the kind gift of EZH2 antibody for coimmunoprecipitation experiments. This study was supported by Science Foundation Ireland (SFI), the Irish Research Council (IRC), and the Fighting Blindness Foundation. The authors declare no conflicts of interest.

AUTHOR CONTRIBUTIONS

D. Andrews carried out the experimental work, analyzed the data, and wrote the manuscript; G. Oliviero carried out the experimental work presented in Fig. 1; L. DeChiara, A. Watson, E. Rochford, C. Kennedy, S. Clerkin, B. Doyle, and K. Wynne also performed experimental work; J. Crean designed and supervised the study with assistance from G. Cagney and D. Andrews and wrote and edited the manuscript; and P. O'Connell, C. O'Brien, and C. Godson edited the manuscript.

REFERENCES

1. Akhurst, R. J., and Hata, A. (2012) Targeting the TGFβ signalling pathway in disease. *Nat. Rev. Drug Discov.* **11**, 790–811
2. Lamouille, S., Xu, J., and Derynck, R. (2014) Molecular mechanisms of epithelial-mesenchymal transition. *Nat. Rev. Mol. Cell Biol.* **15**, 178–196
3. Mullen, A. C., Orlando, D. A., Newman, J. J., Lovén, J., Kumar, R. M., Bilodeau, S., Reddy, J., Guenther, M. G., DeKoter, R. P., and Young, R. A. (2011) Master transcription factors determine cell-type-specific responses to TGF-β signaling. *Cell* **147**, 565–576
4. Monteiro, R., Pinheiro, P., Joseph, N., Peterkin, T., Koth, J., Repapi, E., Bonkhofer, F., Kirmizitas, A., and Patient, R. (2016) Transforming growth factor β drives hemogenic endothelium programming and the transition to hematopoietic stem cells. *Dev. Cell* **38**, 358–370
5. Derynck, R., and Zhang, Y. E. (2003) Smad-dependent and Smad-independent pathways in TGF-beta family signalling. *Nature* **425**, 577–584
6. Gaarenstroom, T., and Hill, C. S. (2014) TGF-β signaling to chromatin: how Smads regulate transcription during self-renewal and differentiation. *Semin. Cell Dev. Biol.* **32**, 107–118
7. Cao, R., Wang, L., Wang, H., Xia, L., Erdjument-Bromage, H., Tempst, P., Jones, R. S., and Zhang, Y. (2002) Role of histone H3 lysine 27 methylation in Polycomb-group silencing. *Science* **298**, 1039–1043
8. Czermin, B., Melfi, R., McCabe, D., Seitz, V., Imhof, A., and Pirrotta, V. (2002) Drosophila enhancer of Zeste/ESC complexes have a histone H3 methyltransferase activity that marks chromosomal polycomb sites. *Cell* **111**, 185–196
9. Bernstein, B. E., Mikkelsen, T. S., Xie, X., Kamal, M., Huebert, D. J., Cuff, J., Fry, B., Meissner, A., Wernig, M., Plath, K., Jaenisch, R., Wagschal, A., Feil, R., Schreiber, S. L., and Lander, E. S. (2006) A bivalent chromatin structure marks key developmental genes in embryonic stem cells. *Cell* **125**, 315–326
10. Brookes, E., de Santiago, I., Hebenstreit, D., Morris, K. J., Carroll, T., Xie, S. Q., Stock, J. K., Heidemann, M., Eick, D., Nozaki, N., Kimura, H., Ragoussis, J., Teichmann, S. A., and Pombo, A. (2012) Polycomb associates genome-wide with a specific RNA polymerase II variant, and regulates metabolic genes in ESCs. *Cell Stem Cell* **10**, 157–170
11. Estarás, C., Akizu, N., García, A., Beltrán, S., de la Cruz, X., and Martínez-Balbás, M. A. (2012) Genome-wide analysis reveals that Smad3 and JMJD3 HDM co-activate the neural developmental program. *Development* **139**, 2681–2691
12. Bertero, A., Brown, S., Madrigal, P., Osnato, A., Ortmann, D., Yiangou, L., Kadiwala, J., Hubner, N. C., de Los Mozos, I. R., Sadée, C., Lenaerts, A. S., Nakanoh, S., Grandy, R., Farnell, E., Ule, J., Stunnenberg, H. G., Mendjan, S., and Vallier, L. (2018) The SMAD2/3 interactome reveals that TGFβ controls m^6A mRNA methylation in pluripotency. *Nature* **555**, 256–259
13. Du, D., Katsuno, Y., Meyer, D., Budi, E. H., Chen, S. H., Koeppen, H., Wang, H., Akhurst, R. J., and Derynck, R. (2018) Smad3-mediated recruitment of the methyltransferase SETDB1/ESET controls *Snail1* expression and epithelial-mesenchymal transition. *EMBO Rep.* **19**, 135–155
14. Faherty, N., Curran, S. P., O'Donovan, H., Martin, F., Godson, C., Brazil, D. P., and Crean, J. K.et al(2012) CCN2/CTGF increases expression of miR-302 microRNAs, which target the TGFβ type II receptor with implications for nephropathic cell phenotypes. *J. Cell Sci.* **125**, 5621–5629
15. Faherty, N., O'Donovan, H., Kavanagh, D., Madden, S., McKay, G. J., Maxwell, A. P., Martin, F., Godson, C., and Crean, J.et al(2013) TGFβ and CCN2/CTGF mediate actin related gene expression by differential E2F1/CREB activation. *BMC Genomics* **14**, 525
16. De Chiara, L., Andrews, D., Watson, A., Oliviero, G., Cagney, G., and Crean, J. (2017) miR302 regulates SNAI1 expression to control mesangial cell plasticity. *Sci. Rep.* **7**, 42407, erratum: 46802
17. Oliviero, G., Brien, G. L., Waston, A., Streubel, G., Jerman, E., Andrews, D., Doyle, B., Munawar, N., Wynne, K., Crean, J., Bracken, A. P., and Cagney, G. (2016) Dynamic protein interactions of the polycomb repressive complex 2 during differentiation of pluripotent cells. *Mol. Cell Proteomics* **15**, 3450–3460
18. Heninger, A.-K., and Buchholz, F. (2007) Production of endoribonuclease-prepared short interfering RNAs (esiRNAs) for specific and effective gene silencing in mammalian cells. *CSH Protoc.* **2007**, pdb.prot4824
19. Shechter, D., Dormann, H. L., Allis, C. D., and Hake, S. B. (2007) Extraction, purification and analysis of histones. *Nat. Protoc.* **2**, 1445–1457
20. Smith, C. M., Gafken, P. R., Zhang, Z., Gottschling, D. E., Smith, J. B., and Smith, D. L. (2003) Mass spectrometric quantification of acetylation at specific lysines within the amino-terminal tail of histone H4. *Anal. Biochem.* **316**, 23–33
21. Feller, C., Forné, I., Imhof, A., and Becker, P. B. (2015) Global and specific responses of the histone acetylome to systematic perturbation. *Mol. Cell* **57**, 559–571
22. Turriziani, B., Garcia-Munoz, A., Pilkington, R., Raso, C., Kolch, W., and von Kriegsheim, A. (2014) On-beads digestion in conjunction with data-dependent mass spectrometry: a shortcut to quantitative and dynamic interaction proteomics. *Biology (Basel)* **3**, 320–332
23. Cox, J., and Mann, M. (2011) Quantitative, high-resolution proteomics for data-driven systems biology. *Annu. Rev. Biochem.* **80**, 273–299
24. Cao, Q., Yu, J., Dhanasekaran, S. M., Kim, J. H., Mani, R. S., Tomlins, S. A., Mehra, R., Laxman, B., Cao, X., Yu, J., Kleer, C. G., Varambally, S., and Chinnaiyan, A. M. (2008) Repression of E-cadherin by the polycomb group protein EZH2 in cancer. *Oncogene* **27**, 7274–7284
25. Casari, A., Schiavone, M., Facchinello, N., Vettori, A., Meyer, D., Tiso, N., Moro, E., and Argenton, F. (2014) A Smad3 transgenic reporter reveals TGF-beta control of zebrafish spinal cord development. *Dev. Biol.* **396**, 81–93
26. Liu, L., Liu, X., Ren, X., Tian, Y., Chen, Z., Xu, X., Du, Y., Jiang, C., Fang, Y., Liu, Z., Fan, B., Zhang, Q., Jin, G., Yang, X., and Zhang, X. (2016) Smad2 and Smad3 have differential sensitivity in relaying TGFβ signaling and inversely regulate early lineage specification. *Sci. Rep.* **6**, 21602

27. Peinado, H., Quintanilla, M., and Cano, A. (2003) Transforming growth factor beta-1 induces snail transcription factor in epithelial cell lines: mechanisms for epithelial mesenchymal transitions. *J. Biol. Chem.* **278**, 21113–21123
28. Smits, A. H., Jansen, P. W., Poser, I., Hyman, A. A., and Vermeulen, M. (2013) Stoichiometry of chromatin-associated protein complexes revealed by label-free quantitative mass spectrometry-based proteomics. *Nucleic Acids Res.* **41**, e28
29. Callahan, J. F., Burgess, J. L., Fornwald, J. A., Gaster, L. M., Harling, J. D., Harrington, F. P., Heer, J., Kwon, C., Lehr, R., Mathur, A., Olson, B. A., Weinstock, J., and Laping, N. J. (2002) Identification of novel inhibitors of the transforming growth factor beta1 (TGF-beta1) type 1 receptor (ALK5). *J. Med. Chem.* **45**, 999–1001
30. Tan, J., Yang, X., Zhuang, L., Jiang, X., Chen, W., Lee, P. L., Karuturi, R. K., Tan, P. B., Liu, E. T., and Yu, Q. (2007) Pharmacologic disruption of polycomb-repressive complex 2-mediated gene repression selectively induces apoptosis in cancer cells. *Genes Dev.* **21**, 1050–1063
31. Miranda, T. B., Cortez, C. C., Yoo, C. B., Liang, G., Abe, M., Kelly, T. K., Marquez, V. E., and Jones, P. A. (2009) DZNep is a global histone methylation inhibitor that reactivates developmental genes not silenced by DNA methylation. *Mol. Cancer Ther.* **8**, 1579–1588
32. Verma, S. K., Tian, X., LaFrance, L. V., Duquenne, C., Suarez, D. P., Newlander, K. A., Romeril, S. P., Burgess, J. L., Grant, S. W., Brackley, J. A., Graves, A. P., Scherzer, D. A., Shu, A., Thompson, C., Ott, H. M., Aller, G. S., Machutta, C. A., Diaz, E., Jiang, Y., Johnson, N. W., Knight, S. D., Kruger, R. G., McCabe, M. T., Dhanak, D., Tummino, P. J., Creasy, C. L., and Miller, W. H. (2012) Identification of potent, selective, cell-active inhibitors of the histone lysine methyltransferase EZH2. *ACS Med. Chem. Lett.* **3**, 1091–1096
33. Vincent, T., Neve, E. P., Johnson, J. R., Kukalev, A., Rojo, F., Albanell, J., Pietras, K., Virtanen, I., Philipson, L., Leopold, P. L., Crystal, R. G., de Herreros, A. G., Moustakas, A., Pettersson, R. F., and Fuxe, J. (2009) A SNAIL1-SMAD3/4 transcriptional repressor complex promotes TGF-beta mediated epithelial-mesenchymal transition. *Nat. Cell Biol.* **11**, 943–950
34. Tong, Z. T., Cai, M. Y., Wang, X. G., Kong, L. L., Mai, S. J., Liu, Y. H., Zhang, H. B., Liao, Y. J., Zheng, F., Zhu, W., Liu, T. H., Bian, X. W., Guan, X. Y., Lin, M. C., Zeng, M. S., Zeng, Y. X., Kung, H. F., and Xie, D. (2012) EZH2 supports nasopharyngeal carcinoma cell aggressiveness by forming a co-repressor complex with HDAC1/HDAC2 and Snail to inhibit E-cadherin. *Oncogene* **31**, 583–594
35. Herranz, N., Pasini, D., Díaz, V. M., Francí, C., Gutierrez, A., Dave, N., Escrivà, M., Hernandez-Muñoz, I., Di Croce, L., Helin, K., García de Herreros, A., and Peiró, S. (2008) Polycomb complex 2 is required for E-cadherin repression by the Snail1 transcription factor. *Mol. Cell. Biol.* **28**, 4772–4781
36. Tien, C. L., Jones, A., Wang, H., Gerigk, M., Nozell, S., and Chang, C. (2015) Snail2/Slug cooperates with polycomb repressive complex 2 (PRC2) to regulate neural crest development. *Development* **142**, 722–731
37. Barroso-del Jesus, A., Lucena-Aguilar, G., and Menendez, P. (2009) The miR-302-367 cluster as a potential stemness regulator in ESCs. *Cell Cycle* **8**, 394–398
38. Kim, S. W., Yoon, S. J., Chuong, E., Oyolu, C., Wills, A. E., Gupta, R., and Baker, J. (2011) Chromatin and transcriptional signatures for Nodal signaling during endoderm formation in hESCs. *Dev. Biol.* **357**, 492–504
39. Yoon, S. J., Foley, J. W., and Baker, J. C. (2015) HEB associates with PRC2 and SMAD2/3 to regulate developmental fates. *Nat. Commun.* **6**, 6546
40. Yoshitake, Y., Howard, T. L., Christian, J. L., and Hollenberg, S. M. (1999) Misexpression of Polycomb-group proteins in Xenopus alters anterior neural development and represses neural target genes. *Dev. Biol.* **215**, 375–387
41. Cano, A., Pérez-Moreno, M. A., Rodrigo, I., Locascio, A., Blanco, M. J., del Barrio, M. G., Portillo, F., and Nieto, M. A. (2000) The transcription factor snail controls epithelial-mesenchymal transitions by repressing E-cadherin expression. *Nat. Cell Biol.* **2**, 76–83
42. Lin, Y., Dong, C., and Zhou, B.P. (2014) Epigenetic regulation of EMT: the Snail story. *Curr. Pharm. Deds.* **20**, 1968–1705
43. Javaid, S., Zhang, J., Anderssen, E., Black, J. C., Wittner, B. S., Tajima, K., Ting, D. T., Smolen, G. A., Zubrowski, M., Desai, R., Maheswaran, S., Ramaswamy, S., Whetstine, J. R., and Haber, D. A. (2013) Dynamic chromatin modification sustains epithelial-mesenchymal transition following inducible expression of Snail-1. *Cell Rep.* **5**, 1679–1689
44. Subramanyam, D., Lamouille, S., Judson, R. L., Liu, J. Y., Bucay, N., Derynck, R., and Blelloch, R. (2011) Multiple targets of miR-302 and miR-372 promote reprogramming of human fibroblasts to induced pluripotent stem cells. *Nat. Biotechnol.* **29**, 443–448
45. Rada-Iglesias, A., Bajpai, R., Swigut, T., Brugmann, S. A., Flynn, R. A., and Wysocka, J. (2011) A unique chromatin signature uncovers early developmental enhancers in humans. *Nature* **470**, 279–283
46. Zentner, G. E., Tesar, P. J., and Scacheri, P. C. (2011) Epigenetic signatures distinguish multiple classes of enhancers with distinct cellular functions. *Genome Res.* **21**, 1273–1283
47. Kloet, S. L., Makowski, M. M., Baymaz, H. I., van Voorthuijsen, L., Karemaker, I. D., Santanach, A., Jansen, P. W. T. C., Di Croce, L., and Vermeulen, M. (2016) The dynamic interactome and genomic targets of Polycomb complexes during stem-cell differentiation. *Nat. Struct. Mol. Biol.* **23**, 682–690

Received for publication May 24, 2018.
Accepted for publication January 22, 2019.